Applied Thermal Engineering 219 (2023) 119454

Contents lists available at ScienceDirect

Applied Thermal Engineering

journal homepage: www.elsevier.com/locate/apthermeng

Research Paper

Module-based simulation model for prediction of convective and condensational heat recovery in a centrifugal wet scrubber

Wanja Johansson [a], Jun Li [b], Leteng Lin [a,*]

[a] Department of Built Environment and Energy Technology, Linnaeus University, Sweden
[b] Department of Chemical and Process Engineering, University of Strathclyde, United Kingdom

ARTICLE INFO

Keywords:
Simulation model
Heat recovery
Centrifugal wet scrubber
Condensation
Biomass
Combustion

ABSTRACT

Biomass combustion is a carbon–neutral method to generate heat and power and is integral to combating climate change. The wet scrubber is a promising device for recovering heat and reducing particle emissions from flue gas, under the driving force of new European Union legislation. Here, the heat recovery of a wet scrubber was investigated using process data and computer simulations. The process data showed that the scrubber could continuously recover heat corresponding to 10–20% of the energy input. The simulation model consists of two interlinked modules: Module 1 simulates droplet movement in the scrubber, while Module 2 uses the output of Module 1 to predict the heat recovery. The model was validated against process data, showing a mean error of 5.6%. Further optimization was based on the validated model by varying different process parameters, including nozzle position and moisture addition to the flue gas. Moisture addition was shown to be a feasible strategy for potentially increasing heat recovery by up to 3.3%. These results indicate that heat recovery in wet scrubbers is a feasible way to make particle removal cost effective in medium-scale combustion facilities, and that the developed simulation model can play an important role in optimizing these processes.

1. Introduction

Biomass combustion is a carbon–neutral method to produce heat and electricity and is therefore integral to the energy transition needed to mitigate climate change [1]. Over the last 40 years, the use of biomass for energy has increased threefold in Sweden, reaching a supply of 145 TWh in 2021 [2]. However, biomass combustion will always lead to emissions of particulate matter, which is harmful to human health [3,4]. There are several well-established processes to remove particulate matter from flue gas, including electrostatic precipitation, bag filtration, and wet scrubbing. However, for economic reasons, it has not been commonplace to use these processes in small- and medium-scale plants; instead, cyclones have been the most widely used alternative [5]. In coming years, stricter European Union (EU) regulations will be enforced, demanding more complete particle removal than cyclones are capable of. Therefore, new alternatives must be developed for the 143,000 medium-scale combustion plants currently operating in the EU [6,7].

Wet scrubbing is a promising application that can recover heat while reducing particle emissions from flue gas. This process step is advantageous if coupled with wet-wood-chip–fired boilers in which up to 30 % of the waste heat can be recovered, due to the high energy content of water vapor [3]. The heat-recovery capacity offered by wet scrubbers can increase their economic feasibility by decreasing the fuel demand of the facility. Studies conducting the simulation modeling of centrifugal wet scrubbers are scarce. Two such studies [8,9] focus on particle collection and flow behavior in the scrubber, but do not consider heat recovery; they were conducted using commercial computational fluid dynamics (CFD) software. A Eulerian–Eulerian method is used in the study determining flow behavior, while a Eulerian–Lagrangian approach is used to determine particle removal. Although not considering flue-gas cleaning, several studies have examined heat recovery from waste flue gas. Veidenbergs et al. investigated the physical parameters of flue gas cooling by evaporation, followed by heat recovery through condensation in a boiler connected to a district heating system [10]; although insightful in its theoretical claims, this study conducted no experimental validation. Maalouf et al. investigated, both experimentally and analytically, heat recovery through direct contact condensation, highlighting the difficulties in recovering the latent heat in flue gases due to the low temperatures at which condensation begins [11]. Regarding the combination of flue gas cleaning and heat recovery, Han et al. investigated the possibility of coupling NOx removal with waste heat recovery, achieving feasible results [12]. Cui et al. developed

* Corresponding author.
E-mail addresses: leteng.lin@lnu.se, leteng.lin@gmail.com (L. Lin).

https://doi.org/10.1016/j.applthermaleng.2022.119454
Received 23 June 2022; Received in revised form 13 September 2022; Accepted 5 October 2022
Available online 17 October 2022

Nomenclature

Roman letter symbols

a	Acceleration
A	Area
Cp	Heat capacity
Cd	Resistance coefficient
d	Diameter
D	Diffusion coefficient
e_a^{21}	Approximate relative error of grid independence
e_{ext}^{21}	Extrapolated relative error of grid independence
E_{vap}	Enthalpy of vaporization
g	Gravity constant
ΔH_{Net}	Net heating value
ΔH_{Gross}	Gross heating value
J	Diffusion flux
k_{order}	Model order for grid independence

Greek letter symbols

δ_{BL}	Width of boundary layer
θ	Extrapolated value for heat recovery
η	Efficiency
ρ	Density
τ	Residence time
Ψ	Heat recovery

Abbreviations

crd	Coordinate
GCI_{fine}	Fine grid convergence index
MCP	Medium-sized combustion plant
WFGR	Water-to-flue-gas ratio
Re	Reynolds number
Sc	Schmidt number
m	Mass
M	Molecular weight
N	Effective number of droplet parcels
p	Pressure
P	Boiler load
q	Grid refinement factor
Q r	Heat transfer Radius
t	Time
T	Temperature
u	Velocity
V	Volume
x	Mass fraction
X	Absolute humidity

a mathematical model for determining heat recovery in a spray tower [13]. A one-dimensional flow was assumed for the gas and droplets, after which a mass and energy balance was determined throughout the tower using an iterative approach. The model was validated against measured data with satisfactory results. Similarly, Men et al. [14] developed a one-dimensional mathematical model to predict heat recovery in three spray towers connected in series with prediction errors below 10 %.

Aside from wet-wood-chip boilers, natural-gas–fired boilers are also feasible for waste heat recovery through condensation due to the high hydrogen content of their fuel [15]. Terhan et al. [16] investigated heat recovery by a flue gas condenser using a one-dimensional finite-difference method. The study showed good potential for the developed condenser, but the method was not validated. Wei et al. [17] investigated heat recovery and NOx reduction in a vapor pump system. The study showed a potential increase in system efficiency of over 10 %, while reducing NO and NOx emissions by up to 25.4 and 27.8 %, respectively. Waste heat recovery can also be accomplished with an absorption heat pump. This process differs from condensers in that it recovers latent heat through absorption rather than condensation. However, the spray droplets which are in direct contact with the flue gas makes it relevant for comparison with the process studied in this paper. Using a two-dimensional model, Wei et al. [18] studied waste flue gas heat recovery in an open-cycle absorption heat pump. The model was validated as having good accuracy and the device showed potential to increase system efficiency by up to 11 %. However, the model assumed that the flue gas moved only horizontally, and that the absorber solution moved only vertically, assumptions that would limit investigations of more complex geometries. An open cycle absorption heat pump for heat recovery was also modelled by Yang et al. [19]. An Eularian-Lagrangian approach was used, assuming a strictly vertical gas flow which is not affected by the water spray. Despite its simplified gas flow, the model showed good accuracy with errors below 5 %.

It is clear from earlier studies that the recovery of waste process heat has good potential. However, no studies have been found that investigate the feasibility of waste heat recovery in cleaning devices for particle removal. This neglect is likely due to the current omission of heat recovery in most particle removal devices. To better understand the opportunities and challenges offered by heat recovery in flue-gas cleaning devices, investigating the processes governing heat transfer would be of significant interest. However, to investigate devices with more complex geometries than a regular spray tower, highly simplified models such as those used previously [13,14,17] would likely not work. Instead, one could use CFD software, producing models that are far more complex and generally computationally demanding. This is why a model with a medium level of complexity could be of great interest for investigations of such devices.

In this study, a module-based simulation model with a simplified gas flow has been developed and validated against process data from two scrubbers located at district heating plants in Kosta and Överum, Sweden. In addition, heat recovery over time was analyzed in two facilities located in Överum, Sweden and Studsgård, Denmark. Although the investigation of particle removal would also be of interest, this study is limited to investigating heat recovery. Through registered data from process monitoring and investigations with a developed model, the following research questions will be answered: What are the main parameters affecting the heat recovery in wet scrubbers? To what extent can a simplified approach to simulation modeling achieve sufficient accuracy while reducing the computational load?

1.1. Scrubbers for the case study

To increase the economic feasibility of particle removal in medium-scale combustion plants (MCPs), ITK Envifront AB has developed a novel type of centrifugal scrubber incorporating heat recovery. This study investigates three such scrubbers connected to district heating plants located in Kosta and Överum, Sweden and Studsgård, Denmark. The three scrubbers vary in size but operate according to the same principle, as follows. First, the flue gas is accelerated into the scrubber, which is shaped like two opposing flattened cones. A nozzle bank with 25 full-cone spray nozzles at different heights is placed in the center of the scrubber. As the water is ejected from the nozzles in the form of droplets, it is accelerated toward the scrubber wall by the centrifugal force of the flue gas. On their way towards the walls, the droplets capture particles while being heated by the flue gas, mainly through convection and condensation. The scrubber water is then collected and led through a heat exchanger, preheating the returned district heating water and thereby increasing the overall efficiency of the entire system. A

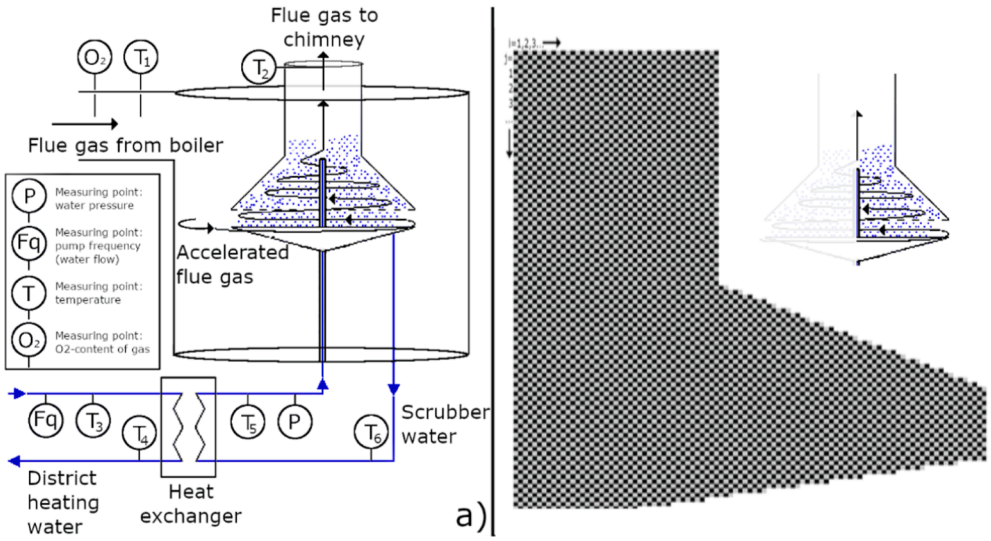

Fig. 1. a) Schematic diagram of a heat-recovery scrubber. b) Mesh generated for simulation model.

Table 1
Measuring devices for process data.

Measuring point	Measuring device
T1	Rotronic HygroFlex 5 Transmitter HF5 HC2
T2	Rotronic HygroFlex 5 Transmitter HF5 HC2A
T3, T4, T5, T6	Pentronic 7941000–149
P	Siemens Sitrans P220
Fq	ABB ACS580
O_2	High frequency O_2-sensor

schematic diagram of the scrubber is shown in Fig. 1a.

The values used for validation and process analysis are process data measured at the points marked in Fig. 1a. The measuring device used at each point is listed in Table 1.

2. Model description (methodology)

To model the scrubber's heat recovery, a script with two interlinked modules was developed in Matlab 2021b. A flow chart of these modules and their connection to each other is shown in Fig. 2. In the first module, the droplet movement in the scrubber was simulated using a Lagrangian approach. The inputs to this module were boiler load, fuel properties, water-to-flue-gas ratio (WFGR), inlet spin velocity of the flue gas, and the height setting of the nozzle bank. This module generated the outputs heat conduction area and water mass flow throughout the scrubber. These outputs were then used as inputs to module two, in which mass and energy balances were calculated throughout the scrubber. The outputs of this module were the temperature distribution throughout the scrubber and the predicted heat recovery from the scrubber. Note that the model was developed to permit adjustment of geometries and nozzle configurations; however, the present validation and investigation are limited to the configurations and geometries of the scrubbers presented in Section 1 under their relevant operating conditions.

2.1. Module 1: Droplet simulation

In this module, the droplet movement through the scrubber was simulated. In the droplet simulation, scrubber symmetry was assumed and the simulation was performed in three dimensions. However, only two dimensions were recorded for calculations in Module 2, in order to decrease the computational load. Fig. 1b shows the 2D mesh in which the droplet information was stored. In the rest of the text, each element will be referred to according to the height segment, *i*, and width segment, *j*, to which it belongs. The simulated height of both scrubbers was 0.8 m. The scrubber radius was 0.3 m in Överum and 0.4 m in Kosta. Note that only half the scrubber was modeled and that symmetry was assumed in the horizontal plane.

A flow chart of the droplet simulation is shown in Fig. 2 and will be further explained below. First, the calculated parameters, including velocity, volume, and position, were entered for the simulated droplet. Second, the new velocity and coordinates of the droplet were calculated, after which the droplet's interactions with other droplets in the scrubber were determined. The current position, volume, and velocity of the droplet were then recorded for further use in Module 2. The program then determined whether the droplet had hit the scrubber wall or left the scrubber. If one of these conditions was true, this was recorded and the simulation of the current droplet ended; if not, the earlier steps were repeated. All these steps will be examined in detail in the following sections.

2.1.1. Droplet generation

At each moment in time, a wet scrubber will contain billions of droplets. Calculating the trajectory of each would demand extreme computational resources and was therefore considered unworkable. Instead, the generally accepted approach is to simulate a limited number of droplets taken to represent the behavior of the actual number of droplets present in the scrubber. These simulated droplet groups are called droplet parcels. The number of droplets that each parcel represents is referred to as the effective number.

According to the nozzle manufacturer, the mean droplet diameter was expected to be 750 μm at a water pressure of 0.7 Bar. However, the droplet size is significantly reduced at higher water pressures, and the actual droplet size can be estimated with Eq. (1):

$$d_{\text{drop}} = 750 \bullet \left(\frac{0.7}{p_{\text{water}}}\right)^{0.3} \quad (1)$$

The droplet size distribution was assumed to follow a normal distribution pattern [20]. However, to reduce the computational load and increase stability, the size range was limited to that within which 95 % of the mass was expected to be found.

2.1.2. Droplet movement

The velocity when the droplets leave the nozzle can be calculated as a function of the area of the nozzle opening and the water volume flow:

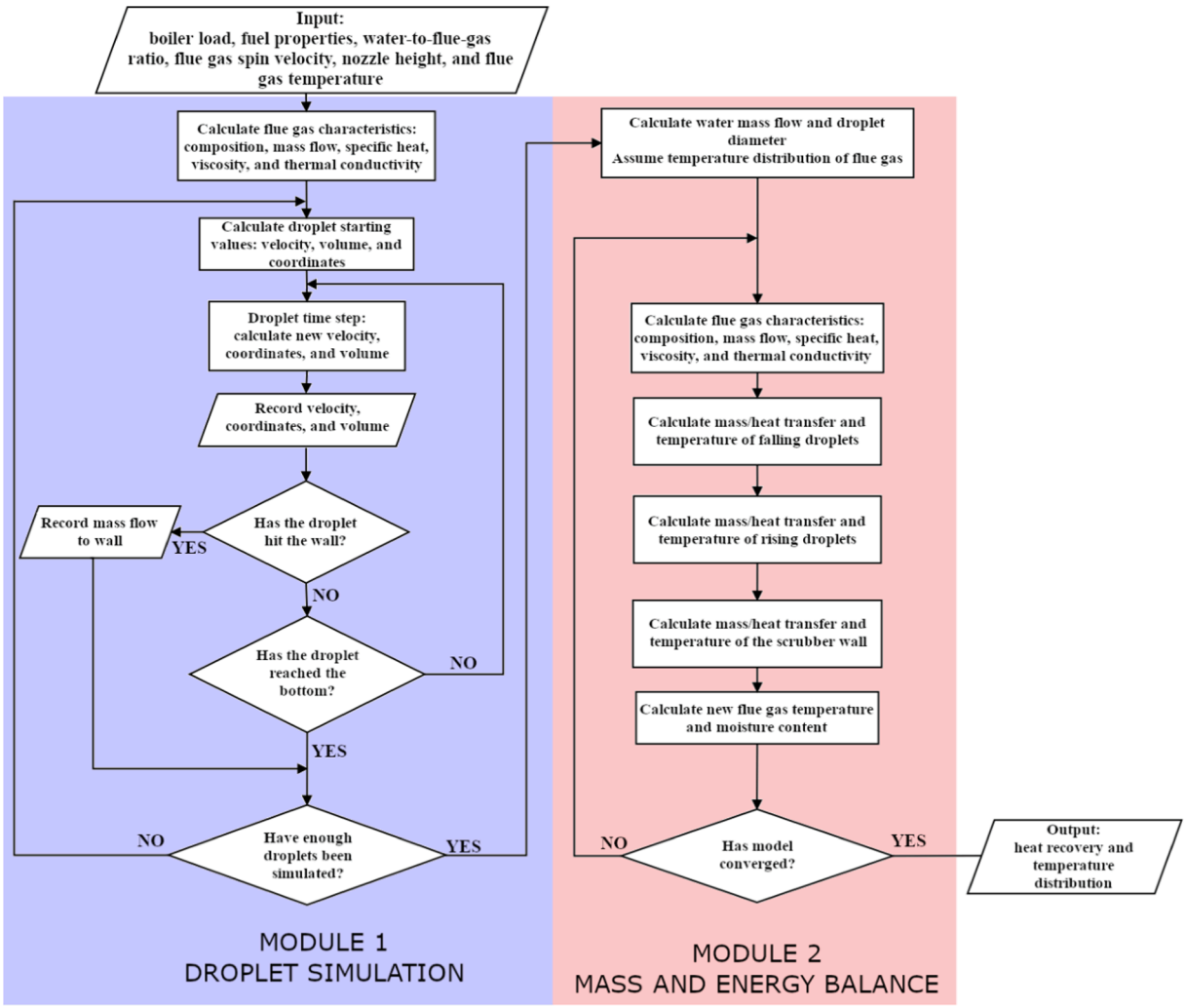

Fig. 2. Flow chart of scrubber model.

$$u_{\text{start}} = \frac{\dot{V}}{A_{\text{nozzle}}} \tag{2}$$

where $\dot{V}$ is the water volume flow and A_{nozzle} the area of the nozzle opening.

When the droplets move through the scrubber, three main forces that affect their velocity are gravity, buoyancy, and the drag force from the flue gas. The acceleration due to drag can be expressed by Eq. (3) [21]:

$$a_{\text{drag}} = \frac{C_{\text{d}} \bullet \rho_{\text{gas}} \bullet {d_{\text{drop}}}^2 \bullet \pi \bullet u_{\text{rel}} \bullet |u_{\text{rel}}|}{m_{\text{drop}} \bullet 8} \tag{3}$$

where ρ_{gas} is the gas density, d_{drop} the droplet diameter, u_{rel} the droplet velocity relative to the gas, m_{drop} the droplet mass, and C_{d} a resistance coefficient, calculated by:

$$C_{\text{d}} = \frac{24}{Re} \text{ for } Re < 1.9 \tag{4}$$

$$C_{\text{d}} = \frac{18.5}{Re^{0.6}} \text{ for } 1.9 \leq Re \leq 508 \tag{5}$$

$$C_{\text{d}} = 044 \text{ for } 508 \leq Re \leq 200,000 \tag{6}$$

The acceleration due to gravity and buoyancy is calculated with Eq. (7):

$$a_{\text{drag}} = \frac{{d_{\text{drop}}}^3 \bullet \pi \bullet (\rho_{\text{drop}} - \rho_{\text{gas}})}{6 \bullet m_{\text{drop}}} \bullet g \tag{7}$$

The new velocity in the $\times$ and y directions is then described by Eq. (8):

$$\frac{\text{du}}{\text{dt}} = a_{\text{drop}} \tag{8}$$

Then, a new droplet position can be calculated with Eq. (9):

$$crd_{\text{new}} = crd_{\text{old}} + u_{\text{new}} \bullet \Delta t \tag{9}$$

2.1.3. Mass flow averaging

To account for the different ages and temperatures of the droplets in a single scrubber segment, the total water mass flow in the scrubber was treated as the sum of three separate mass flows of rising droplets, falling droplets, and the wall's liquid film, respectively. Whenever a droplet moved between two volume segments, a new mass flow was recorded as described by Eq. (10):

$$\dot{m}_{\text{i}} = \sum m_{\text{drop}} \bullet N_{\text{droplet}} \tag{10}$$

where $\dot{m}_{\text{i}}$ is the water mass flow, m_{drop} the mass of each simulated droplet moving through the segment, and N_{droplet} the effective number of droplet parcels.

When the droplets reach the wall, they are assumed to form a film flowing down the wall. This film was not simulated, but the mass flow at

Table 2
Fuel and flue-gas composition for modeling the reference scenario.

Fuel composition	**Mass fraction**
H_2O	50 $\%_{wet}$
C	51 $\%_{dry}$
O	43 $\%_{dry}$
H	6 $\%_{dry}$
Flue gas component	**Molar** $\%_{wet}$
N_2	61.4
O_2	4.6
CO_2	22.7
H_2O	11.3

each height segment was approximated from the number of droplets reaching the wall. This mass flow was found from a mass balance according to Eq. (11):

$$\dot{m}_{i+1} = \dot{m}_i + \dot{m}_{droplets} \tag{11}$$

where $\dot{m}_i$ is the film mass flow coming into height segment i, $\dot{m}_{i+1}$ the film mass flow leaving height segment i, and $\dot{m}_{droplets}$ the mass flow of droplets reaching the wall.

2.1.4. Surface area of droplets

To find the surface area available for heat transfer in each scrubber segment, the residence water volume must be found. This was calculated according to Eq. (12):

$$V_{res} = \frac{\dot{V}}{\overline{\tau}} \tag{12}$$

where V_{res} is the residence volume of droplets, $\dot{V}$ the droplet volume flow, and $\overline{\tau}$ the mean residence time of the droplets.

The heat transfer area was then calculated with Eq. (13):

$$A = V_{res} \bullet \frac{V_{drop}}{A_{drop}} = V_{res} \bullet \frac{r_{drop}}{3} \tag{13}$$

where V_{drop} is the mean volume of droplets, A_{drop} the mean surface area of droplets, and r_{drop} the mean droplet radius in the relevant scrubber segment.

2.1.5. Flue gas characteristics

Both the droplet movement and the heat transfer between droplets and flue gas will be widely affected by the flue gas composition and movement. This section will describe how the flue gas composition and properties were determined in the model. First, the boiler load, boiler efficiency, and fuel properties were used to determine the fuel input into the boiler according to Eqs. (14) and (15). The fuel used in the case study facilities was woodchips and an estimation of its properties was obtained from the Phyllis database [22].

$$\Delta H_{Net} = \Delta H_{Gross} - 2.443\,\hat{A}\cdot\left\{8.936\frac{x_H}{100} \bullet \left(1 - \frac{x_{H_2O}}{100}\right) + \frac{x_{H_2O}}{100}\right\} \tag{14}$$

$$\dot{m}_{fuel} = \frac{P}{\Delta H_{Net}} \bullet \eta_{Boiler} \tag{15}$$

where ΔH_{Net} is the net calorific value, ΔH_{Gross} the gross calorific value, x_H the mass percentage of hydrogen on a dry ash-free basis, x_{H_2O} the mass percentage of water on a wet basis, $\dot{m}_{fuel}$ the fuel input, P the boiler load, and η_{Boiler} the boiler efficiency.

The composition and mass flow of flue gas were calculated through a stoichiometric analysis of the combustion. In this study, complete combustion was assumed, and the presence of SO_X was omitted due to its extremely low concentration from woody biomass combustion and its negligible influence on the heat recovery. The flue gas composition will vary between different scenarios depending on the fuel moisture and the air supply to the boiler. However, for the process optimization, a reference scenario was determined in which the air factor was assumed to be 1.4 and the fuel moisture content 50 %. These values were chosen according to the running condition of the boiler in the case study. The fuel composition and the corresponding flue gas composition in the base scenario are shown in Table 2.

The viscosity, thermal conductivity, and specific heat of the individual flue gas components were calculated according to the polynomial models used in the literature [23–25]. Wilke's model was used to calculate the viscosity of the whole gas mixture [26], and Lindsay and Bromley's model was used to calculate the thermal conductivity of the whole gas mixture [27]. The specific heat of the gas mixture was calculated with Eq. (16):

$$Cp_{mixture} = \sum Cp \bullet x \tag{16}$$

where Cp and $\times$ are the specific heat and mass fraction of each gas component, respectively.

To reduce the computational load, the current model uses a simplified flow pattern in the scrubber. The gas velocity was divided into a horizontal and a vertical component. Before entering the contact zone, the gas is accelerated. Assuming no losses, the total velocity of the gas as it enters the contact zone can be calculated with Eq. (17):

$$u_{tot} = \sqrt{\frac{2 \bullet p_{drop}}{\rho_{gas}}} \tag{17}$$

where u_{tot} is the total gas velocity, P_{drop} the pressure drop in the inlet, and ρ_{gas} the density of the gas as it enters the scrubber.

The horizontal velocity component was assumed to be perpendicular to the scrubber wall at every point. The vertical velocity was calculated as a function of the volume flow and cross-sectional area at each given height; see Eq. (18):

$$u_{vert} = \frac{\dot{V}}{A} \tag{18}$$

2.2. Module 2: Mass and energy balances

In the second module, the outputs of Module 1 were used to establish the mass and energy balances throughout the scrubber. The main relevant modes of heat transfer are convection and condensation; although radiation is low at the investigated temperatures, it is still accounted for in the model.

For the convective heat transfer, a model suggested by Ahmed and Yovanovich was used for the droplets [28], and Hausen's formula for gas flows in pipes and canals was used for the scrubber wall film [29]. Leckner's gray gas model was used for the radiation [30]. For the droplet sizes relevant to this study, the rate of heat transfer within the droplets was expected to be so much faster than the heat transfer between droplets and flue gas that it can be assumed to be instantaneous.

For the condensation of vapor on droplets and walls, Lock's model [31] and a modified version of Nusselt's film theory [32] can be used, respectively. However, due to the presence of non-condensable gases in the gas mixture, the diffusion of water vapor must be considered as well. The interaction between gas and water will occur through the boundary layer of the droplet. At the water surface, the temperature of the gas can be assumed to be the same as that of the water. At an increasing distance from the droplet, the gas temperature increases until it reaches the ambient gas temperature. This phenomenon was earlier described by Veidenberg et al. [10]. At the water surface, the vapor pressure can be assumed to be the saturation pressure at a given temperature. The rate of vapor diffusion can therefore be calculated with Eq. (19) [32]:

$$J = -D \bullet \frac{p_{sat}(T_{FG}) - p_{sat}(T_{water})}{\delta_{BL}} \tag{19}$$

where D is the diffusion coefficient of vapor in the gas, p_{sat} the saturation pressure of vapor at a given temperature, and δ_{BL} the width of the droplet's boundary layer, which was calculated with Eq. (20):

$$\delta_{BL} = \frac{d_{droplet}}{2 + Re^{0.5} \bullet Sc^{0.375}} \quad (20)$$

where Re is the Reynolds number and Sc the Schmidt number.

The saturation pressures at different temperatures were calculated according to the Antoine equation with constants gathered from Stull [33].

The mass flow due to condensation can then be calculated with Eq. (21), while the heat transfer can be calculated with Eq. (22):

$$\dot{m}_{diff} = J \bullet A_{surface} \bullet M_{H_2O} \quad (21)$$

$$Q_{cond} = \dot{m}_{diff} \bullet E_{vap} \quad (22)$$

where $\dot{m}_{diff}$ is the mass flow due to condensation or evaporation, M_{H_2O} the molar mass of water, $A_{surface}$ the surface area of the droplets, and E_{vap} the enthalpy of vaporization for water.

The mass balance of the scrubber water was calculated according to Eq. (23), and the new temperature was calculated according to Eq. (24):

$$\dot{m}_{w_{out}} = \dot{m}_{w_{in}} + m_{condensed} - m_{evaporated} \quad (23)$$

$$T_{drop_{out}} = T_{drop_{in}} + \frac{Q_{conv} + Q_{cond}}{\dot{m}_{w_{out}} \bullet Cp_{H_2O}} \quad (24)$$

where $\dot{m}_w$ is the mass flow of water into and out of the scrubber segment, T_{drop} the droplet temperature, P_{Conv} the convective heat transfer, and Cp_{H_2O} the specific heat of water.

Considering the simplified flow field described above, it makes little sense to calculate mass and heat balances in two dimensions for the flue gas. Instead, only one dimension was considered, extending from top to bottom. Therefore, the heat recovery and condensation calculated above were summed for each height segment, as shown in Eqs. (25)–(26):

$$m_{condensed_{tot}} = \sum_{j}^{Y} m_{condensed_j} \quad (25)$$

where $m_{condensed_{tot}}$ is the total amount of water condensed at a given height, Y the total number of scrubber segments in the horizontal direction, and $m_{Condensed_j}$ the condensation at each individual scrubber segment at a given height.

$$Q_{tot_i} = \sum_{j}^{N} Q_{ij} \quad (26)$$

where Q_{tot_i} is the total heat transfer at a given height, N the total number of scrubber segments in the horizontal direction, and Q_{ij} the heat transfer in each width segment, j, and height segment, i.

Using the calculated heat/mass transfer as well as the mass flow and temperature of incoming water, a mass and energy balance can be established. After this, the new moisture content and temperature of each scrubber segment were calculated with Eqs. (27)–(28):

$$X_i = X_{i+1} - \frac{m_{condensed_{tot}}}{m_{dryFG}} \quad (27)$$

where X is the absolute humidity in kg of vapor per kg of dry gas.

$$T_{out} = \frac{\dot{m}_{FGin} \bullet Cp_{FGin} \bullet \left(T_{FGin} - T_{ref}\right) + \dot{m}_{FGout} \bullet Cp_{FGout} \bullet T_{ref} + \dot{m}_{cond_{tot}} \bullet Cp_{vapor} \bullet T_{ref} - P_{tot_i}}{\dot{m}_{FGin} {}^{*} Cp_{FGin} + \dot{m}_{condensed_{tot\,i}} \bullet Cp_{vapor}} \quad (28)$$

2.3. Moisture addition

Earlier studies have investigated the potential advantages of increasing the moisture content of the flue gas before it enters the scrubber [10]. The possibility of investigating these advantages was therefore included in the non-equilibrium model. The theory behind this is explained below.

The moisture was assumed to be added by spraying small amounts of water into the flue gas, water that evaporates before the gas reaches the scrubber. Considering the actual process, this water addition could also be realized by combusting fuel with a higher moisture content. This would decrease the temperature of the flue gas while increasing its moisture content and dew point. The new temperature and moisture content of the flue gas can be calculated with Eqs. (29)–(31):

$$\Delta E = Cp_{H_2O} \bullet m_{moist} \bullet \left(T_{dew} - T_{W_{in}}\right) + m_{moist} \bullet \Delta E_{Vap} + Cp_{vapor} \bullet m_{moist} \bullet \left(T_{out} - T_{dew}\right) \quad (29)$$

where ΔE is the energy needed to vaporize the added water, m_{moist} the water added to the flue gas, T_{dew} the dew point of the flue gas, T_W the temperature of the inserted water, Cp the specific heat, and T_{gas} the final temperature of the flue gas.

$$T_{out} = T_{FGin} - \frac{\Delta E}{Cp_{FGout} \bullet \dot{m}_{FGout}} \quad (30)$$

$$X_{out} = X_{in} + \frac{m_{moist}}{m_{FG\,dry}} \quad (31)$$

In principle, the theoretical maximum amount of moisture that could be added to the flue gas would be reached when the new flue gas temperature equaled the dew point. The model was therefore tested with moisture additions of 0–100 % of this theoretical maximum.

Table 3
Calculation of the discretization error.

Y1	120,000
Y2	60,000
Y3	30,000
$q_{21} = q_{32}$	1.4
Ψ_1	353.1
Ψ_2	353.7
Ψ_3	353.5
k_{order}	3.99
θ_{ext}^{21}	351.4
e_a^{21}	0.19 %
e_{ext}^{21}	0.47 %
GCI_{fine}^{12}	0.59 %

2.4. Numerical solving methods

Given the great complexity of mass flows in the scrubber, there are too many unknown temperatures in each scrubber segment to be able to solve the energy balances analytically. A numerical solution was therefore proposed and applied. First, an arbitrary temperature profile of the flue gas was assumed as a starting input. The heat exchange between the flue gas and the water was then calculated, and an energy balance was set up in each segment, solving for the water temperature profile. The calculated mass and heat exchange were then used to calculate a new temperature profile of the flue gas as well as a profile of the flue gas composition. This process was then iterated until the model converged to a solution. Convergence was assumed to be reached when the total energy balance between water and flue gas checked out, and the heat recovery had changed less than 1 % over the last 400 iterations.

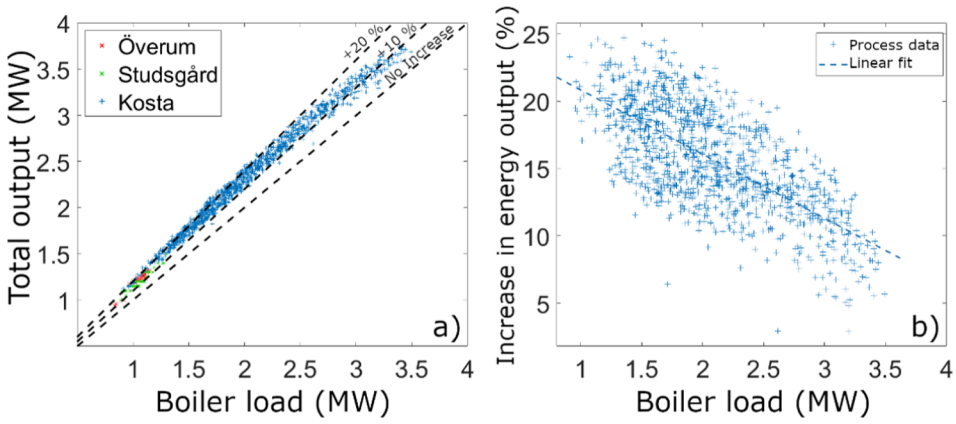

Fig. 3. Energy output to district heating with installed scrubber versus the energy output without heat recovery.

The predicted heat recovery was calculated as the mean of the last 200 iterations. To facilitate convergence, an under-relaxation factor of 0.5 was used for the mass and energy balance. This value was then successively reduced for 200 iterations until it reached 0. To ensure that the under-relaxation did not alter the final results, the software did not start to check for convergence until 400 iterations had passed.

3. Model validation

3.1. Grid independence

As mentioned above, the developed model solved the mass and energy balances in two dimensions for the water flow, while only one dimension was used for the flue gas. To ensure grid independence, the discretization error of the heat recovery was determined according to the well-established method proposed by Celik et al. [34]. Table 3 shows the input and results of the grid independence investigation. N is the number of elements in each trial, chosen so that the grid refinement factor, q, would be 1.4. For each grid size, the heat recovery was determined. This showed that the order, k_{order}, of the method was 3.99. The extrapolated value for the heat recovery (when the number of elements goes to infinity) was 351.4 kW. The approximate relative error, e_a^{21}, was 0.19 %, the extrapolated relative error, e_{ext}^{21}, was 0.47 %, and the fine grid convergence index, GCI_{fine}^{12}, was 0.59 %. These values indicate that the grid size has only a small impact on the predicted heat recovery. Note that the results may indicate an oscillatory convergence of the model. However, due to the small differences in calculated heat recovery between the different grids, this could be deemed acceptable. As a compromise between computational load and accuracy, a grid size of 80,000 elements was chosen.

Another sensitive factor that may affect the simulation results is the number of simulated droplets. Pretests were performed to find the optimal number to use by varying the number of simulated droplets between 1000 and 500,000. Simulations conducted with fewer than 50,000 droplets displayed fluctuations of up to 2 % in the predicted heat recovery. When the number of simulated droplets was increased further, the fluctuations stopped and the predicted heat recovery flattened out. As the predictions with 100,000 and 500,000 droplets differed by less than 0.1 %, the number of simulated droplets was set to 100,000 in this study.

3.2. Validation against process data

The model validation was performed using process data from two sources: a scrubber installed in the 1990 s in Överum, and a similar scrubber in 2018 in Kosta. Process data were gathered from these facilities and used as input for the developed model. The predicted heat recovery was then compared with the heat recovery at each corresponding data point.

Since the moisture content of the fuel input at each time point was unknown, it had to be estimated from the data available. This was done by calculating an energy balance for the scrubber using the increase in scrubber water temperature, incoming and outgoing flue gas temperatures, and the mass flow of flue gas.

4. Results and discussion

4.1. Heat recovery in case study facilities.

To increase the economic viability of wet scrubbers in MCP facilities, the scrubbers in the case study were designed to recover the flue gas

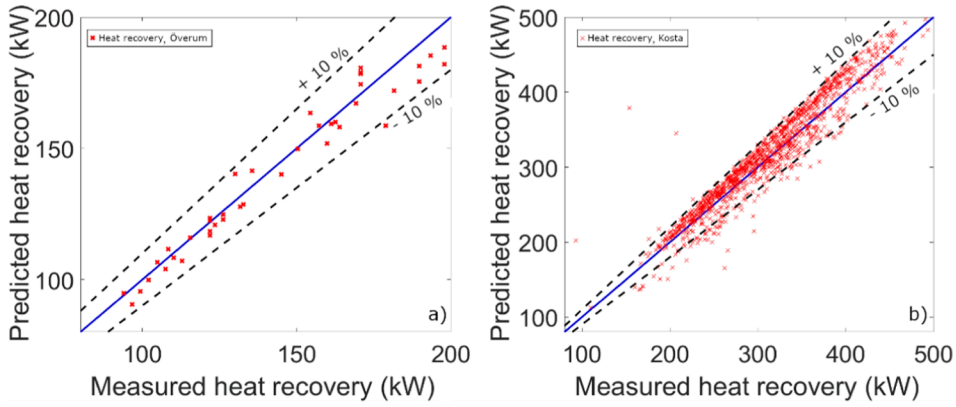

Fig. 4. Comparison of model predictions and process data for heat recovery by the scrubber installations in a) Överum and b) Kosta.

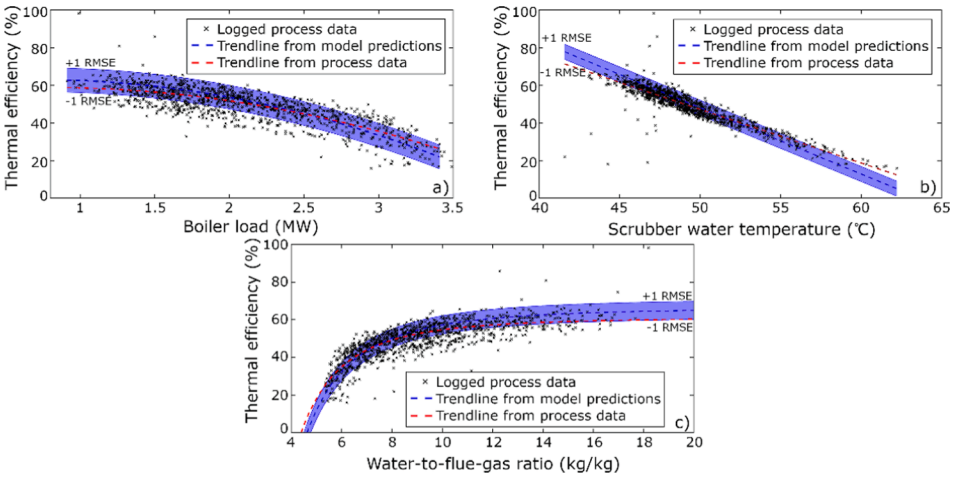

Fig. 5. Effects of process parameters on thermal efficiency. Trend lines are fitted to the process data and model predictions. The band shows the model trend line ± 1 root mean squared error (RMSE).

energy by means of convection and condensation. To investigate the benefits of this, the heat recovery was logged at 88 time points over two days at the Studsgård and Överum facilities and at 1176 time points over 12 months at the Kosta facility. The heat recovery was then evaluated against the boiler heat output at each time point. As shown in Fig. 3a, evaluation of the process data from the facilities shows that the heat recovered by the scrubber increased the energy that the facility could deliver to the district heating system by an average of 15 %. This suggests that the system could lead to significant fuel savings at the facilities, which could pay for some of the installation costs, making the scrubbers more economically viable. Note, however, that the relative increase is negatively correlated to boiler load (see Fig. 3b), suggesting that optimization may be needed if scrubbers are used at higher boiler loads. The large variation in the data is likely due to variations in process conditions over the measurement period. Several parameters linked to the heat recovery in the scrubber also fluctuate significantly over the year. First, the fuel moisture content is directly linked to the vapor available for condensation in the scrubber. Second, the air factor affects the thermal efficiency of the scrubber by means of the increased mass flow and reduced humidity of the flue gas. Third, the return temperature of the district heating water is a factor limiting how much heat can be recovered. Finally, scrubber operating conditions, such as water supply and nozzle configuration, have specific effects on the heat recovery. Due to their possible significance for the process, these parameters will be further investigated in Section 4.3.

4.2. Model validation

Although the insights gained from simulation models can be of great interest, it is crucial that a model should be validated against experimental data before any conclusions are drawn from its predictions. The model developed here was therefore validated against process data from two different facilities, in Kosta and Överum, Sweden. The measured values of process parameters were used as model input to predict the heat recovery; those predicted values were then compared with the measured heat recovery values.

Validation showed that the model has good predictive accuracy, with a mean prediction error of 3.5 % for the scrubber in Överum (see Fig. 4a) and of 5.6 % for the scrubber in Kosta (see Fig. 4b). This could be compared with prediction errors of 7–15 % for the water temperature in a spray tower studied by Cui et al. [13], below 5 % in an open-cycle absorption heat pump studied by Yang et al. [19], below 10 % in a ceramic membrane studied by Zhang et al. [35], and of below 7.3 % in a compact heat exchanger studied by Shi et al. [36].

To further establish the predictive capacity of the model, the process data from Kosta were analyzed in more detail. The observed effects on the thermal efficiency of changes in process parameters were compared with the effects of these changes established from the scrubber model. The thermal efficiency was defined as the ratio between the recovered heat and the available heat when cooling the flue gas to 25 °C. Trend lines were fitted to the thermal efficiencies calculated from process data and to those obtained from the model. The process data derive from actual operating conditions at the facility, where several process parameters are often changed simultaneously, explaining the large scattering of the data points. To account for this, the standard deviation of the modeled trend line was also plotted. The results of this analysis are shown in Fig. 5a–c and will be further discussed below.

As shown in Fig. 5a, an increase in the boiler load is negatively correlated with the thermal efficiency. This trend can be seen in both the process data and the model predictions. This is also consistent with the negative correlation between the boiler load and the relative increase in energy output shown in Fig. 3b. Fig. 5b shows a negative correlation between the incoming scrubber water temperature and the thermal efficiency. This trend can be seen in both the process data and the model predictions, although the steeper trend line suggests that the model somewhat overestimates the effect. This effect was expected, because an increase in water temperature will inhibit heat exchange, especially at a lower flue gas temperature. This drastic effect is likely because condensation mainly occurs at lower temperatures (less than60℃) and because condensation of the flue gas vapor represents approximately 40 % of the energy recovered from the flue gas. The WFGR, on the other hand, is positively correlated with the thermal efficiency (see Fig. 5c). The trend increases sharply at low WFGRs, leveling off at a WFGR of around 10. Although the same main trend is seen in both the model predictions and the process data, the trends start to diverge at high WFGRs. This is likely caused by the high flexibility of the power function used for the trendline and by the lack of data points under these conditions. The increase in thermal efficiency is expected both as an effect of an increase in the scrubber water available for heat transfer, and because higher water pressure will lead to smaller droplets, which means a larger surface area per water volume unit. The fact that these trends could also be predicted by the model is a good indication of its predictive capacity.

To evaluate the computational time, the model was run and timed for 40 different scenarios on a laptop equipped with an Intel® Core™ i5-10210U processor and 16 GB ram. The mean computational time for one simulation was 2.5 min, much less than what is normally required by CFD models.

Table 4
Scrubber properties investigated with the model.

Flue gas properties	Minimum	Maximum
Fuel moisture (%)	35	55
Inlet water temperature (°C)	40	60
Water-to-flue-gas ratio (kg water/kg flue gas)	5	15
Height of nozzle bank (mm from lowest setting)	0	100
Scrubber hat opening (mm)	80	120
Moisture addition (% of theoretical maximum)	0	100

4.3. Process optimization

As shown above, the validation results suggest that the model could be used with confidence to investigate the possible effects of changes in different scrubber parameters. Therefore, the model was used to study the effects on scrubber efficiency of varying different process parameters. These parameters were investigated by adjusting one parameter at a time while keeping the other parameters constant. The investigated parameters and the range over which they were evaluated were chosen according to the current operating conditions of the scrubber modeled here and are shown in Table 4; the results of these investigations are shown in Fig. 6.

An increase of 1 % in the moisture content of the fuel increases the thermal efficiency by approximately 1 % (see Fig. 6a). This is because the increased vapor content of the flue gas leads to a higher dew point and more condensation. This corresponds well with the finding that condensational heat-recovery devices such as this are more feasible for facilities combusting wet fuels [3].

The inlet water temperature was an important parameter determining the heat recovery (see Fig. 6b). This was expected, as a lower water temperature allows a larger decrease in the flue gas temperature in the scrubber. The importance of this parameter was also recognized by Yang et al. [19], and Zhang et al. [36]. However, this is not a parameter that is easily changed, since it is connected to the return temperature of the district heating water, which is generally kept as low as the system allows.

Changes in the WFGR produced a significant increase in the thermal efficiency up to a value of around 12, after which the increase seemed to level off (see Fig. 6c). Increased efficiency due to increased water injection is to be expected, since more droplets will be present in the scrubber. However, as the efficiency increases, the temperature of the outgoing flue gas approaches that of the scrubber water, making further increases in efficiency harder to achieve. An increase in water supply will also lead to a lower final droplet temperature, which will lead to problems in the heat exchanger between the scrubber and the district heating water.

Adjusting the nozzle height produced small differences in thermal efficiency (see Fig. 6d). The highest efficiency was achieved when the nozzle bank was set to 60 mm above the lowest setting, but the efficiency differed by only approximately 0.8 % compared with that in the lowest setting, which gave the worst performance.

Increasing the opening of the scrubber hats produced a maximum efficiency increase of 0.8 % (see Fig. 6e), attributable to an increased contact volume between the droplets and the flue gas. However, note that adjusting the opening is likely to affect the flue gas flow and velocity, which cannot be accounted for with the simplified flue gas flow used in this model.

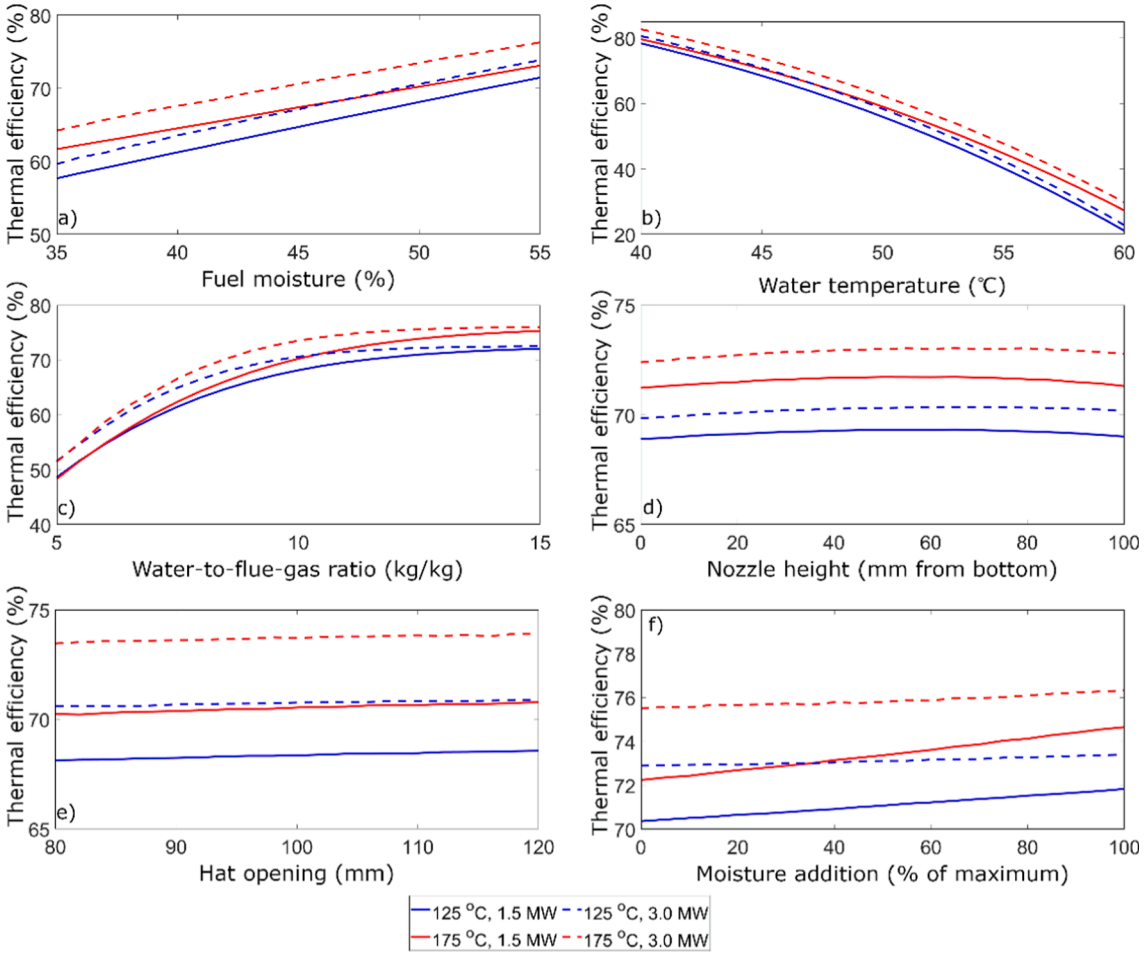

Fig. 6. Correlation between thermal efficiency and process parameters.

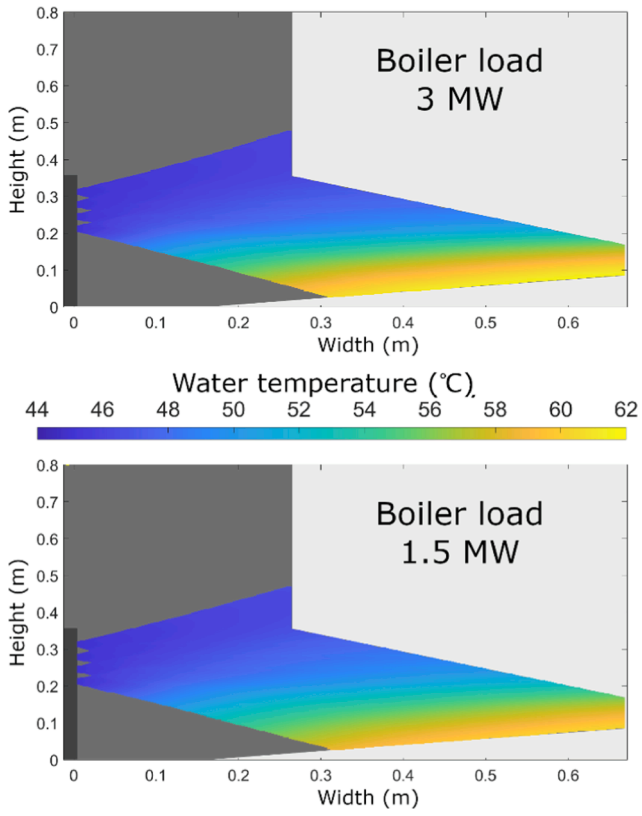

Fig. 7. Simulated water temperature distribution in scrubber.

Moisture addition to the flue gas showed the potential to increase heat recovery by up to 3.3 %, with larger increases occurring at higher flue gas temperatures (see Fig. 6f). Although the theoretical maximum may not be achieved in an actual process, the notable efficiency increase predicted by the model indicates that it would be of interest to further investigate moisture addition. The efficiency increase can be attributed to the moisture addition enhancing condensation in the scrubber, shifting the dominant type of heat transfer in the scrubber from convection to condensation. As condensation is generally a more effective type of heat transfer than is convection, this will lead to increased heat recovery in the scrubber. This effect correlates well with Veidenberg et al.'s [10] suggestion.

4.4. Temperature distribution in scrubber

Fig. 7 shows the temperature distribution of the scrubber droplets at boiler loads of 1.5 and 3 MW, respectively. As expected, the water temperature increases steadily as the water moves downwards and outwards through the scrubber. Since the water injection is directly proportional to the flue gas flow, similar temperatures are reached even though the incoming energy in the flue gas is doubled in the full-load compared with the half-load case.

It can be also observed that the final water temperature is higher in the 3 MW case. This implies higher thermal efficiency in the higher-load case, which is in agreement with the indications in Fig. 6. This notable effect is likely due to the relationship between water injection and droplet size. At a constant WFGR, the higher flue gas flow leads to more injected water. This is related to a reduced droplet size (approximately 260 μm at 3 MW and 400 μm at 1.5 MW) and thereby to a larger droplet surface area per volume unit, facilitating heat recovery. This effect can be contrasted to the trend shown in Fig. 5a, in which increased boiler load was related to decreased thermal efficiency. This is explained by the fact the facility operates at a constant water injection rate rather than a constant WFGR.

5. Conclusions

One way to increase the economic feasibility of centrifugal wet scrubbers is to incorporate heat recovery in the scrubbing process. In this study, the potential to incorporate heat recovery in centrifugal scrubbers was investigated using process data from three full-scale facilities as well as by developing a module-based simulation model, building on numerical methods.

The process data from the facilities showed that the investigated process had good potential to increase the thermal efficiency of the facilities, with heat recovery reaching 15 % of the boiler load. The simulation model developed here showed that these benefits could be further enhanced by optimizing the scrubbing process. The developed simulation model deepened our understanding of the heat transfer phenomena within the scrubber. The two most important parameters affecting thermal efficiency were fuel moisture content and inlet water temperature. An increase of 1 % in fuel moisture led to an increase of approximately 1 % in thermal efficiency. Due to reduced condensation, increased inlet water temperature decreased the thermal efficiency by almost 6 % for every degree of increase. However, since these parameters are not easily regulated, moisture addition to the incoming flue gas was also suggested, with potential to increase the heat recovery by approximately 3 %.

This model can predict general trends regarding the effects of process parameters on heat transfer with a reasonable margin of error of approximately 5.6 %. The model does not compete with the CFD approach when it comes to accuracy and spatial resolution. However, it has low computational demands and quickly produces results, making it feasible as an engineering tool or a predictor embedded in a control system. It is also believed that it could be used as a complementary research tool, scanning a wide set of process configurations so that CFD investigations could focus on the more promising ones.

CRediT authorship contribution statement

Wanja Johansson: Conceptualization, Methodology, Software, Validation, Formal analysis, Investigation, Data curation, Writing – original draft, Visualization. **Jun Li:** Writing – review & editing. **Leteng Lin:** Conceptualization, Resources, Supervision, Project administration, Funding acquisition, Formal analysis, Writing - review & editing.

Declaration of Competing Interest

The authors declare that they have no known competing financial interests or personal relationships that could have appeared to influence the work reported in this paper.

Data availability

The authors do not have permission to share data.

Acknowledgements

The authors wish to acknowledge a grant from the Swedish Knowledge Foundation (project number 20190090). We thank ITK Envifront AB for its support, especially Fredrik Albertson and Staffan Jansson for their useful input. We also thank Lessebo Fjärrvärme for its support, especially Mike Lundström and Mikael Fredh for their useful input.

References

[1] P. Z. V. Masson-Delmotte, H. O. Pörtner, D. Roberts, J. Skea, P.R. Shukla, A. Pirani, W. Moufouma-Okia, C.Péan, R. Pidcock, S. Connors, J. B. R. Matthews, Y. Chen, X. Zhou, M. I. Gomis, E. Lonnoy,T. Maycock, M. Tignor, T. Waterfield (eds.), "Summary for Policymakers. In:Global warming of 1.5°C. An IPCC Special Report on the impacts of global warming of 1.5°C above pre-industrial levels and related global greenhouse gas emission pathways, in the context of strengthening the

global response to the threat of climate change, sustainable development, and efforts to eradicate poverty," 2018. Accessed: Aug. 30, 2022. [Online]. Available: https://www.ipcc.ch/sr15/chapter/spm/.
[2] Swedish Energy Agency, "Energy in Sweden 2021 - an overview," Eskilstuna, 2021. Accessed: Aug. 30, 2022. [Online]. Available: https://energimyndigheten.a-w2m.se/Home.mvc?ResourceId=198022.
[3] S. Van Loo, J. Koppejan, The handbook of biomass combustion and co-firing, Earthscan, London, 2008.
[4] I.M. Kennedy, The health effects of combustion-generated aerosols, Proceedings of the Combustion Institute 31 (2) (2007) 2757–2770, https://doi.org/10.1016/j.proci.2006.08.116.
[5] J. Fagerström, Fine particle emissions and slag formation in fixed-bed biomass combustion: aspects of fuel engineering, Department of Applied Physics and Electronics, Umeå University, 2015. Ph.D. dissertation,.
[6] The European Parliament and the council of the European Union, "Directive (EU) 2015/2193 of the European Parliament and of the Council of 25 November 2015 on the limitation of emissions of certain pollutants into the air from medium combustion plants (Text with EEA relevance)," Brussels, 2015. Accessed: Aug. 30, 2022. [Online]. Available: https://eur-lex.europa.eu/legal-content/GA/TXT/?uri=CELEX:32015L2193.
[7] The European Commission, "Impact assessment Accompanying the documents Communication from the Commission to the Council, the European Parliament, the European Economic and Social Committee and the Committee of the Regions - a Clean Air Programme for Europe," Brussels, 2014. Accessed: Aug. 30, 2022. [Online]. Available: https://eur-lex.europa.eu/legal-content/EN/TXT/?uri=CELEX%3A52013SC0532.
[8] H. Ali, F. Plaza, A. Mann, Flow visualization and modelling of scrubbing liquid flow patterns inside a centrifugal wet scrubber for improved design, Chemical engineering science 173 (2017) 98–109, https://doi.org/10.1016/j.ces.2017.06.047.
[9] H. Ali, F. Plaza, A. Mann, Numerical prediction of dust capture efficiency of a centrifugal wet scrubber, AIChE Journal 64 (3) (2018) 1001–1012, https://doi.org/10.1002/aic.15979.
[10] I. Veidenbergs, D. Blumberga, E. Vigants, and G. Kozuhars, "Heat and Mass Transfer Processes in Scrubber of Flue Gas Heat Recovery Device," *Scientific Journal of Riga Technical University. Environmental and Climate Technologies,* vol. 4, no. -1, 2010, 10.2478/v10145-010-0025-4.
[11] S. Maalouf, E. Boulawz Ksayer, D. Clodic, Investigation of direct contact condensation for wet flue-gas waste heat recovery using Organic Rankine Cycle, Energy conversion and management 107 (2016) 96–102, https://doi.org/10.1016/j.enconman.2015.09.047.
[12] Y. Han, Y. Sun, Collaborative optimization of energy conversion and NOx removal in boiler cold-end of coal-fired power plants based on waste heat recovery of flue gas and sensible heat utilization of extraction steam, Energy (Oxford) 207 (2020), 118172, https://doi.org/10.1016/j.energy.2020.118172.
[13] H. Cui, N. Li, J. Peng, R. Yin, J. Li, Z. Wu, Investigation on the thermal performance of a novel spray tower with upward spraying and downward gas flow, Applied Energy 231 (2018) 12–21, https://doi.org/10.1016/j.apenergy.2018.09.123.
[14] Y. Men, X. Liu, T. Zhang, Performance comparison of different total heat exchangers applied for waste heat recovery, Applied thermal engineering 182 (2021), 115715, https://doi.org/10.1016/j.applthermaleng.2020.115715.
[15] Y. Wang, Q. Zhao, Q. Zhou, Z. Kang, W. Tao, Experimental and numerical studies on actual flue gas condensation heat transfer in a left–right symmetric internally finned tube, International journal of heat and mass transfer 64 (2013) 10–20, https://doi.org/10.1016/j.ijheatmasstransfer.2013.03.005.
[16] M. Terhan, K. Comakli, Design and economic analysis of a flue gas condenser to recover latent heat from exhaust flue gas, Applied thermal engineering 100 (2016) 1007–1015, https://doi.org/10.1016/j.applthermaleng.2015.12.122.
[17] M. Wei, L. Fu, S. Zhang, X. Zhao, Experimental investigation on vapor-pump equipped gas boiler for flue gas heat recovery, Applied thermal engineering 147 (2019) 371–379, https://doi.org/10.1016/j.applthermaleng.2018.07.069.
[18] M. Wei, W. Yuan, Z. Song, L. Fu, S. Zhang, Simulation of a heat pump system for total heat recovery from flue gas, Applied thermal engineering 86 (2015) 326–332, https://doi.org/10.1016/j.applthermaleng.2015.04.061.
[19] B. Yang, Y. Jiang, L. Fu, S. Zhang, Conjugate heat and mass transfer study of a new open-cycle absorption heat pump applied to total heat recovery of flue gas, Applied thermal engineering 138 (2018) 888–899, https://doi.org/10.1016/j.applthermaleng.2018.04.054.
[20] W. Plumecocq, L. Audouin, J.P. Joret, H. Pretrel, Numerical method for determining water droplets size distributions of spray nozzles using a two-zone model, Nuclear engineering and design 324 (2017) 67–77, https://doi.org/10.1016/j.nucengdes.2017.08.031.
[21] M. Rieutord, Fluid dynamics: an introduction, Springer Cham, 2015.
[22] TNO Biobased and Circular Technologies, "Phyllis2, database for (treated) biomass, algae, feedstocks for biogas production and biochar." Accessed: Aug. 30, 2022. [Online]. Available: https://phyllis.nl/.
[23] C.L. Yaws, X. Lin, L. Bu, Viscosity of gas, in: Chemical Properties Handbook, McGraw-Hill, 1999, pp. 452–477.
[24] C. L. Yaws, X. Lin, and L. Bu, "Thermal Conductivity of Gas," in: Chemical Properties Handbook. New York: McGraw Hill, 1999, pp. 505-531.
[25] X. Lin, S. Nijhawan, C. Yaws, D. Balundgi, S. Tripathi, Heat Capacity of Gas. Chemical Properties Handbook, McGraw-Hill, New York, 1999.
[26] C.R. Wilke, A Viscosity Equation for Gas Mixtures, The Journal of Chemical Physics (April 1950) 517–519.
[27] A.L. Lindsay, L.A. Bromley, Thermal Conductivity of Gas Mixtures, Industrial and Engineering Chemistry (August 1950) 1508–1511.
[28] G. Ahmed, M. Yovanovich, Analytical method for forced convection from flat plates, circular cylinders, and spheres, Journal of Thermophysics and Heat Transfer 9 (07/01 1995,) 516–523, https://doi.org/10.2514/3.695.
[29] H. Alvarez, Energiteknik, 3 ed., Studentlitteratur, Lund, 2006.
[30] B. Leckner, Spectral and total emissivity of water vapor and carbon dioxide, Combustion and Flame 19 (1) (1972/08/01/ 1972) 33–48, https://doi.org/10.1016/S0010-2180(72)80084-1.
[31] G.S.H. Lock, Latent Heat Transfer: An Introduction to Fundamentals, Oxford University Press, 1996.
[32] R.B. Bird, W.E. Stewart, E.N. Lightfoot, D.J. Klingenberg, Introductory Transport Phenomena, Wiley, 2015.
[33] D.R. Stull, Vapor Pressure of Pure Substances. Organic and Inorganic Compounds, Industrial and engineering chemistry 39 (4) (1947) 517–540, https://doi.org/10.1021/ie50448a022.
[34] "Procedure for Estimation and Reporting of Uncertainty Due to Discretization in CFD Applications," Journal of Fluids Engineering, 130(7) (2008) 10.1115/1.2960953.
[35] J. Zhang, Z. Li, H. Zhang, H. Chen, D. Gao, Numerical study on recovering moisture and heat from flue gas by means of a macroporous ceramic membrane module, Energy (Oxford) 207 (2020), 118230, https://doi.org/10.1016/j.energy.2020.118230.
[36] X. Shi, D. Che, B. Agnew, J. Gao, An investigation of the performance of compact heat exchanger for latent heat recovery from exhaust flue gases, International journal of heat and mass transfer 54 (1) (2011) 606–615, https://doi.org/10.1016/j.ijheatmasstransfer.2010.09.009.